International Journal of Solids and Structures 47 (2010) 2445–2458

Contents lists available at ScienceDirect

International Journal of Solids and Structures

journal homepage: www.elsevier.com/locate/ijsolstr

Effects of adhesive thickness on global and local Mode-I interfacial fracture of bonded joints

Gefu Ji [a], Zhenyu Ouyang [b], Guoqiang Li [a,b,*], Samuel Ibekwe [b], Su-Seng Pang [a]

[a] Department of Mechanical Engineering, Louisiana State University, Baton Rouge, LA 70803, USA
[b] Department of Mechanical Engineering, Southern University, A&M College, Baton Rouge, LA 70813, USA

ARTICLE INFO

Article history:
Received 21 October 2009
Received in revised form 4 May 2010
Available online 31 May 2010

Keywords:
Cohesive zone model
Bonded joints
Adhesive thickness
Toughness
Plastic zone
Interfacial strength
Cohesive law
Cohesive strength

ABSTRACT

The interfacial fracture of adhesively bonded structures is a critical issue for the extensive applications to a variety of modern industries. In the recent two decades, cohesive zone models (CZMs) have been receiving intensive attentions for fracture problems of adhesively bonded joints. Numerous global tests have been conducted to measure the interfacial toughness of adhesive joints. Limited local tests have also been conducted to determine the interface traction-separation laws in adhesive joints. However, very few studies focused on the local test of effects of adhesive thickness on the interfacial traction-separation laws. Interfacial toughness and interfacial strength, as two critical parameters in an interfacial traction-separation law, have important effect on the fracture behaviors of bonded joints. In this work, the global and local tests are employed to investigate the effect of adhesive thickness on interfacial energy release rate, interfacial strength, and shapes of the interfacial traction-separation laws. Basically, the measured laws in this work reflect the equivalent and lumped interfacial fracture behaviors which include the cohesive fracture, damage and plasticity. The experimentally determined interfacial traction-separation laws may provide valuable baseline data for the parameter calibrations in numerical models. The current experimental results may also facilitate the understanding of adhesive thickness-dependent interface fracture of bonded joints.

1. Introduction

Adhesive bonding technology is being used in a variety of modern industries, including the automotive, aerospace, maritime, construction, defense etc. Many components and structures, from microchips to ships and large aircrafts are made of materials arranged in layers through adhesive bonding. However, early or even some current design approaches (critical stress method) for predicting the failure of adhesively bonded materials are still somewhat empirical. In order to improve prediction ability of these traditional approaches, the interfacial fracture mechanics was introduced for joined substrates which may be identified by the pilot work of Williams (1959) half century ago. In the following three decades, numerous studies had been contributed to failure problems of bonded joints (Hutchinson and Evans, 2000). During this stage, most efforts were focused on the classical linear elastic fracture mechanics (LEFM). The advantage of LEFM lies in the obvious simplicity and decent accuracy, especially for relatively brittle materials and interfaces. Within the framework of LEFM, the remote loadings can be correlated to the critical conditions (crack growth) by a local parameter: stress intensity factor (SIF) or a global parameter: strain energy release rate (ERR). Despite the huge success of LEFM, some limitations have been identified due to the fundamental assumption of LEFM which requires small-scale yielding beyond the crack tip. Specifically, with the increased use of modern toughened adhesives, the plastic zones associated with cohesive fracture along the adhesive interlayer, in many cases, could be comparable to or even larger than the thickness of the adherends.

Motivated by this limitation of LEFM, a number of efforts have been made along the direction of nonlinear fracture mechanics (NLFM). In the late 1950s and early 1960s, on one hand, Barenblatt (1959), Dugdale (1960) independently proposed the concept of cohesive zone. In their idea, the stresses across a potential crack path were bounded, and a localized traction-separation law may be able to describe the fracture behaviors within the cohesive processing zone ahead of the apparent crack tip. The stresses vary with the relative surface separations according to the assumed interface law during the fracture process. On the other hand, in the late 1960s, Rice (1968) proposed a path independent integral method to calculate the energy release rate (ERR), which is referred to as the well-known *J*-integral. For a monotonically loaded process, large-scale bulk inelasticities and nonlinear interfacial cohesive

* Corresponding author at: Department of Mechanical Engineering, Louisiana State University, Baton Rouge, LA 70803, USA. Tel.: +1 225 578 5302; fax: +1 225 578 5924.
E-mail address: guoli@me.lsu.edu (G. Li).

0020-7683/$ - see front matter © 2010 Elsevier Ltd. All rights reserved.
doi:10.1016/j.ijsolstr.2010.05.006

separations might be considered by the *J*-integral method. Encouraged by these two achievements, intensive studies have been conducted to investigate the nonlinear fracture behaviors of adhesively bonded joints for the past three decades. Specially, 1990s might be the most rapidly developing period of CZMs. The realistic demands for nonlinear simulation become urgent due to the wide applications of modern toughened adhesive. With such a situation, the classical LEFM, which is basically a single-parameter method, may have difficulties of meeting the increased demands in the accurate fracture simulations and predictions. Instead of the single-parameter model in LEFM, it has been reported that two or even three parameters were needed in CZMs for the sake of accurate modeling. For instance, these parameters could be chosen as the fracture toughness, the cohesive strength σ_{max}, and/or the characteristic length at which the cohesive tractions vanish (Wei and Hutchinson, 1998; Williams and Hadavinia, 2002; Ouyang and Li, 2009a).

Various cohesive zone models (cohesive laws) were proposed to model the fracture process (Hillerborg et al., 1976; Rose et al., 1983; Needleman, 1987; Tvergaard, 1990; Xu and Needleman, 1993; Camacho and Ortiz, 1996). The main difference between these models lies in the shape of the traction-displacement response, and the parameters used to describe that shape. All of them start from the assumption that one or more interfaces can be defined, where crack propagation is allowed by the introduction of a possible discontinuity in the displacement field. One feature of CZMs is that they can be conveniently incorporated in the traditional finite element analysis (FEA) to model the fracture behaviors in various materials and structures, including adhesive joints (Hillerborg et al., 1976; Needleman, 1987; Tvergaard, 1990; Tvergaard and Hutchinson, 1992; Xu and Needleman, 1993; Corigliano, 1993; Camacho and Ortiz, 1996; Chowdhury and Narasimhan, 2000; Yang et al., 2001a,b; Alfano and Crisfield, 2001;Andruet et al., 2001; Pardoen et al., 2005; Högberg, 2006; Salomonsson and Andersson, 2008; Parrinello et al., 2009; Yan and Shang, 2009; Moura et al., 2009). It is worth noting that CZMs can be also incorporated in analytical models to derive the theoretical solutions for some types of specimens or structures with relatively simple geometries (Klarbring, 1991; Williams and Hadavinia, 2002; Blackman et al., 2003; Pan and Leung, 2007; Ouyang and Li, 2009a,b,c,d; Lorenzis and Zavarise, 2009; Nguyen and Levy, 2009).

There are several CZMs based methods for numerically simulating interfacial fracture problems of adhesive joints. A simple method is that the entire adhesive layer is modeled by a row of interface elements which are characterized by the traction-separation laws during the FEA implementation. This method usually treats the adhesive interlayer as an entirety, and the thin adhesive layer is replaced by a series of interface elements. Note that most analytical solutions share the same methodology. The global behaviors of adherends are correlated through the inserted interface elements. The geometry of the adhesive interlayer may be modeled by a surface. The applicability of this method is obvious for most practical adhesive joints because of the very thin adhesive layer. Due to its obvious simplicity, this method has been widely used in the fracture simulation of adhesive joints. Previous practices indicated that this model could offer a decent simulation when properly calibrated interfacial laws were provided. Although few computational resources were required, some limitations existed with this method: first, clear physical meanings were lost to some extent. This was because physical cohesive separations were usually accompanied with elastoplastic behaviors across the adhesive interlayer, even for relatively brittle adhesives. In other words, "cohesive laws" should be considered as equivalent interfacial traction-separation laws across the entire interlayer. Meanwhile, interfacial laws became dependent on the geometries, such as thickness of the adherend and adhesive. Because they could affect the size of plastic zone and the magnitude of plastic strain, they changed the equivalent interfacial traction-separation laws.

Motivated by this limitation, another category of CZM based numerical methods was proposed to address this issue for the adhesively bonded joints. Instead of idealizing the entire thin interlayer as an interface, the adhesive layer was modeled as an elastoplatic continuum (Tvergaard and Hutchinson, 1996; Wei and Hutchinson, 1998; Madhusudhana and Narasimhan, 2002; Pardoen et al., 2005). In this method, "intrinsic cohesive laws" were embedded, while plastic dissipations were considered by bulk element of adhesive continuum. In these "CZM + elastioplastic continuum" models, terminologies of "intrinsic fracture energy" and "intrinsic cohesive strength" were used. They may be proposed to conceptually distinguish "work of separation" Γ_0 from the plastic energy Γ_p. According to their reported results, the fracture energy was usually several or dozens of times of the "intrinsic fracture energy". Therefore, the authors speculated that the modeled "intrinsic fracture energy" may not necessarily be the true cohesive energy of polymeric materials at molecular level, since the true intrinsic fracture energy at molecular level should be at least magnified by several hundreds or thousands times in order to match the global toughness. Realistically, FEM fracture simulations usually should be phenomenological model based, rather than the truly physical models, unless molecular dynamics (MD) models are considered. Even for MD models, most of them are phenomenological models (based on intermolecular potentials). Therefore, it seems to us that the terms "intrinsic energy" and "intrinsic strength" may be considered as some kinds of modeling parameters for the phenomenological models. Although the modeling scales in "CZM + elastoplastic continuum" models were still much larger than the size required by real physical models by at least two or three orders of magnitude, they were much smaller than that in the simple models discussed in the last paragraph. Effects of external and internal constraints on adhesive layer's plastic dissipations may be considered by this method. Of course more parameters and computations are needed with this method.

Although these two kinds of CZM based methods show considerable difference, parameters in both methods need calibrations by test data. Importantly, due to the effects of adhesive thickness on plastic dissipations, calibrations are highly preferred to be conducted with different thicknesses of adhesive layer. There might be two means for the parameter characterizations: global method and local method. For the global method, one may compare measured global loadings, deflections and toughnesses to those by numerical models embedded with the parameters to be calibrated, at different adhesive thicknesses. The global behaviors of bonded joints have been widely tested with different adhesive thicknesses (Kinloch and Shaw, 1981; Chai, 1988; Chai, 1995; Ikeda et al., 2000; Kafkalidis et al., 2000; Yan et al., 2001; Madhusudhana and Narasimhan, 2002; Lee et al., 2004; Pardoen et al., 2005), to name a few. Their study clearly showed that the fracture energy varies with the thickness of the adhesive layer. On the contrary, fewer attentions have been paid to the local test on the interfacial traction-separation laws across the interlayer. However, this is also a quite important issue. First, it may provide direct thickness-dependent equivalent interfacial laws for simple models. Meanwhile, it can cross-calibrate the parameters required by the "CZM + elastoplastic continuum" model. One may argue that global tests are sufficiently good to calibrate the parameters. We believe that the local separation between the two adherends may be even a more direct, rigorous and reliable means to calibrate the parameters in a numerical model. Several local experimental tests have been conducted on the local interfacial traction-separation laws for bonded joints. For instance, Sørensen (2002), Andersson and Stigh (2004) experimentally determined the interfacial traction-separation laws of bonded joint under Mode-I loadings. Leffler

et al. (2007) experimentally obtained the interfacial traction-separation law of bonded joint under Mode-II loadings. Recently, interfacial traction-separation laws were also tested under mixed mode loadings (Högberg et al., 2007). Most recently, Liechti and his co-workers (2009) conducted a local fracture test to extract the loading rate-dependent traction-separation laws.

These recent efforts on the local test of interfacial traction-separation laws across the adhesive interlayer provided valuable information. Most of them were conducted with a fixed thickness of adhesive layer (Sørensen (2002) tested two thicknesses). As discussed before, in order to more efficiently calibrate the parameters, the local traction-separation laws tests may be desired with different adhesive thicknesses. However, very few tests have been conducted on the thickness-dependent local interfacial traction-separation laws. Among the very few local tests regarding the effects of the adhesive thickness, Kafkalidis et al. (2000) investigated the interfacial fracture by considering three different thicknesses of the adhesive layer. The purpose of the present work is thus to conduct a systematic study and obtain an entire picture about the effects of the adhesive thickness. Not only its effects on the fracture energy, but also its effects on the local interfacial traction-separation laws are investigated. To this end, six typical adhesive thicknesses (varies from 0.09 to 1.0 mm) are investigated. In order to reduce the workload, the thickness of the adherend (steel) remains identical in this work. Note that the steel adherend thickness is designed to be relatively thick to prevent from any plastic deformation. Thus, all the nonlinear behaviors are limited in the adhesive interlayer. For the cases that plastic deformations are involved in the adherends, one may refer to the studies by Yang and Thouless as well as their co-workers (Yang et al., 2001a,b). Both local and global test are conducted simultaneously. With these test results, the dependency of the interface strength and the shape of the constitutive laws on adhesive thickness can be revealed. The current test results may provide valuable test data for the research communities and facilitate the characterization of the parameters required by both of the two CZM based numerical methods discussed before.

2. Theoretical background

Consider a typical double cantilever beam (DCB) specimen as shown in Fig. 1. It is assumed that the adherends are linearly elastic during the entire fracture test process. Strictly, the adhesive material must be nonlinearly elastic during the test. However, for a monotonic loading process (no unloading occurs), the cohesive separation as well as plastic dissipation in the adhesive layer might still be considered by the well-known path independent integral or *J*-integral as follow (Rice, 1968):

$$J = \int_{\Gamma} \left(W dy - T \frac{\partial u}{\partial x} ds \right), \tag{1}$$

where $W(x,y)$ is the strain energy density; x and y are the coordinate directions, $T = n \cdot \sigma$ is the traction vector; $\boldsymbol{n}$ is the normal to the curve or path Γ, $\boldsymbol{\sigma}$ is the Cauchy stress, and $\boldsymbol{u}$ is the displacement vector.

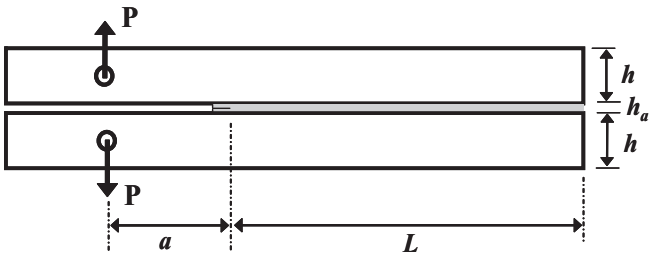

Fig. 1. Schematic of DCB test specimen.

With the *J*-integral theory, based on the concept of energetic force and classical beam theory, Andersson and Stigh (2004) derived a brief expression of *J*-integral for the DCB specimen as follow:

$$J = \frac{(Pa)^2}{D} + P \cdot \theta_0 = P \cdot \theta_P. \tag{2}$$

It is worth noting that the shear effects may become significant for the energy release rate when there is a large-scale fracture zone for conditions such as laminated composite joints. However, for the bonded steel joint with a slender configuration, our preliminary test results showed that the effect of shear deformation was very small (less than 2%). Therefore, the classical beam theory is adopted as shown in Eq. (2).

The interface normal stress can be simply expressed by

$$\sigma(\delta) = \frac{\partial J(\delta)}{\partial \delta}, \tag{3}$$

where J is the energy release rate of the DCB specimen during crack initiation process, P is the global peel load at the loadline, D is the adherend's bending stiffness, θ_0 and θ_P are the relative rotation between the upper and lower adherends at the crack tip and at the loadline, respectively; and δ is the crack tip opening or separation.

With Eqs. (2) and (3), one can see that the energy release rate J can be experimentally determined as the function of the crack tip separation δ if the adhrends' loadline rotation θ_P and the global peel load P are simultaneously recorded as the function of δ during the fracture test. It is important to note that the interfacial normal separation δ represents the opening between the bottom fiber of the upper adherend and the top fiber of the lower adherend. Once the experimental relationship between $J(\delta)$ and δ are obtained, the equivalent interface normal traction $\sigma(\delta)$ can be determined as a function of δ. In other words, the interface constitutive law can be experimentally obtained. It is noted that this interface constitutive relationship is the equivalent interface cohesive law, not necessarily the intrinsic cohesive law. This is because in addition to the intrinsic cohesive separation, possible plastic deformations in the adhesive layer contribute to the entire normal separation between the two adherends during the fracture test. Of course, with the decrease of the adhesive thickness, it is expected that this equivalent interface cohesive law will finally approach the intrinsic cohesive law.

A typical nonlinear equivalent cohesive law is shown in Fig. 2. For most CZMs in the literature, the traction-separation laws are such that with increasing interfacial separation, the traction across the interface reaches a maximum, then decreases and eventually vanishes. This typical nonlinear separation-traction law has three segments: (a) elastic stage when the normal interfacial separation $\delta \leqslant \delta\, B_{0B}$. The normal interfacial stress σ increases with separation until the maximum interfacial stress $\sigma_{\max}$ (interfacial strength) is reached; (b) softening stage when $\delta\, B_{0B} \leqslant \delta \leqslant \delta \mathrm{B}_{fB}$. The normal traction σ decreases with separation δ; and (c) complete debonding stage. There is no interfacial stress when $\delta \geqslant \delta\, \mathrm{B}_{fB}$. By conducting the fracture tests of DCB specimens with different adhesive thicknesses, the effects of adhesive layer on the constitutive laws, such as the interfacial strength, shape of the interfacial traction-separation law, and fracture energy can be revealed.

3. Specimen preparation and experiment set-up

3.1. Raw materials

The adhesive, LOCTITE Hysol 9460, is a modified, thixotropic, and two-component epoxy adhesive. This material has high peel

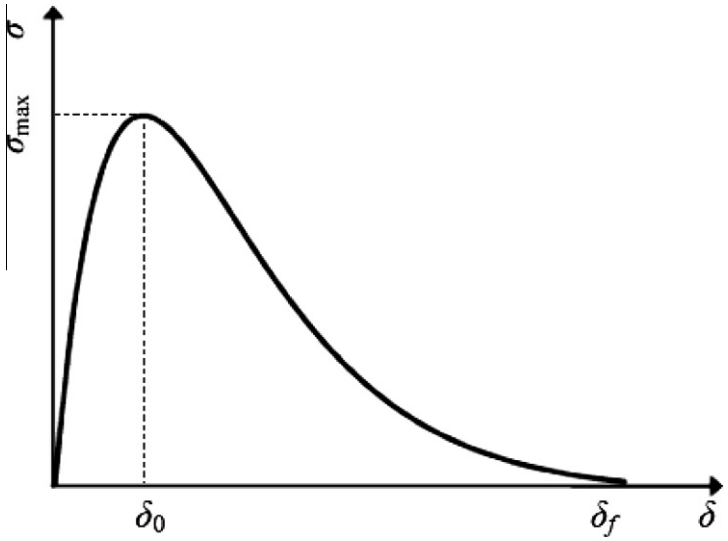

Fig. 2. A typical nonlinear interfacial traction-separation law.

strength, good impact resistant, good fatigue resistant, and is good for bonding metal or dissimilar substrates. The mix ratio of resin and hardener is 1:1 by weight. According to the manufacturer, the tensile strength and elongation is 30.3 MPa and 3.5%, respectively. General purpose 1018 low carbon steel plates with yield strength of 372.3 MPa were used to fabricate the 6.35 mm thick, 25.4 mm wide and 254 mm long adherends of DCB specimens after the cutting, milling, sanding, drilling, and polishing processes.

3.2. Fabrication of double cantilever beam (DCB) specimen

There are two different methods to manufacture the DCBs. One is that the adherends are cut before the adhesive curing processes. The other one is that the two adherends with adhesive experience the curing processes and then are cut to small DCB specimens. The major problem of this method is that during the milling and cutting processes, the adhesive layer could be damaged by metal chips. Therefore, this study cut the adherends before bonding them with adhesive. After cutting, a hole (11.11 mm in diameter), which was 50.8 mm from one end of the adherend, was drilled coaxially in the upper and lower adherends and coaxially machined threads inside the hole to apply the peel load using our specially designed loading fixture as will be discussed later. Once the surface of the adherends was cleaned by using acetone, the adherends were ready for preparing the DCB specimens. The thickness of the adherends was measured before the adhesive was applied and compared with the thickness of the specimen after curing. In order to obtain different and desirable thickness of the adhesive layer, six different thickness feeler gage inserts were inserted in between the two adherends as shown in Fig. 3. The feeler gages can also control the edge of the adhesive and help in keeping the adherends parallel. It is also noted that the surface of the feeler gauges was sprayed with a super-thin layer of mold release agent so that the feeler gauges could be easily removed after the curing. The actual average adhesive thicknesses of the six groups of specimens were 0.09, 0.2, 0.4, 0.6, 0.8, and 1.0 mm, respectively.

A very thin mylar tape with thickness of 0.035 mm was carefully inserted from the edge of the adhesive layer by 2 mm at the middle height of the adhesive layer immediately after the application of the adhesive layer to create a sharp initial crack. Since the distance between the loadline and the edge of the adhesive layer was 50 mm, the total initial crack length "*a*" was 52 mm, as schematically shown in Fig. 4. After the adhesive was applied, a steel pin with the same diameter as the threaded hole was inserted into the hole to hold the adherends in place. The prepared specimens were then pressed by the same weights and cured for 24 h at room temperature. The specimens were further put into an oven at 141 °C for 1 h for post-curing. After that, they were cooled down to room temperature before test.

3.3. Fabrication of self-aligned ball pin

In order to maintain coaxial peel force during the testing, two self-aligned, free-rotating ball pins were designed and fabricated using tool-grade steel, as schematically shown in Fig. 5. One end of the ball pin with threads was mated with the prefabricated threads within the holes in the DCB specimen, and the other end was connected with the MTS machine. The ball pin had an ability

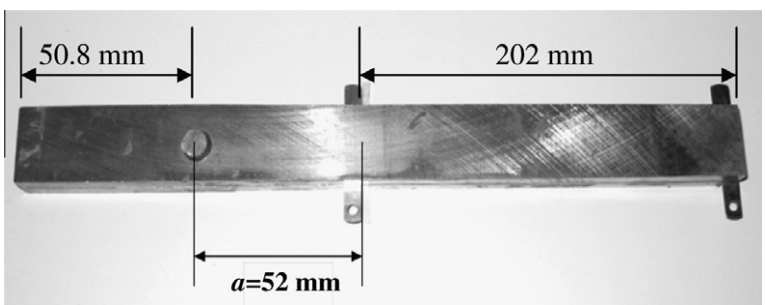

Fig. 3. DCB specimen bonded with polished/cleaned adherends and uniform thickness of adhesive layer through standard feeler gauge.

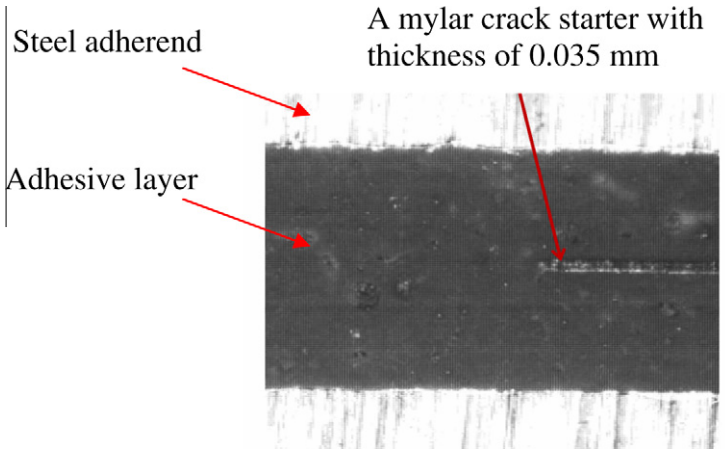

Fig. 4. microscope image shows the inserted 0.035 mm thick mylar sheet located at the middle plane of the adhesive layer.

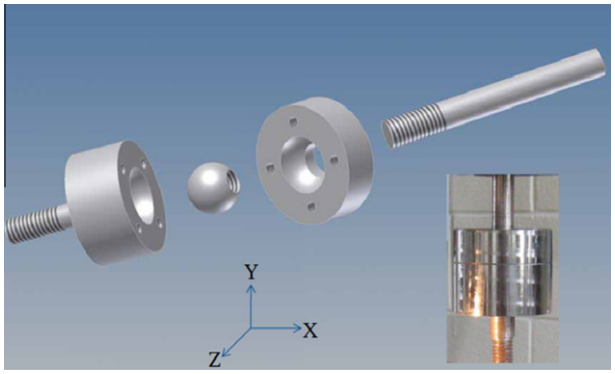

Fig. 5. Schematic of self-aligned free-rotating ball joint.

to rotate 360° in the *XZ* plane and 30° to −30° in the *XY* and *YZ* planes.

3.4. Instrumentation and tensile test

The MTS 810 machine was used to conduct the peel test and collect the loading force data "*P*" and the displacement "Delta" of the DCB specimens at the loading point. The fracture test was conducted under the displacement controlled mode. The loading rate was set as 1 μm/s and the data collecting frequency was 1 Hz. In order to measure the rotating angle "θ" of the adherends during the peel test, two digital inclinometers and sensors were attached at the free end of the adherends to collect the data during the test, as shown in Fig. 6. The accuracy of the inclinometer is 0.01°, the test range is from −70° to 70°, and the data acquisition frequency is 1 Hz. Sony XCD-CR90 High resolution CCD camera with a resolution of 3.7 × 3.7 μm/pixel was used in this experiment. The position of the camera was adjusted to be perpendicular to the side of the DCB specimen and the deformation images of the DCB specimen during the test was shot, with focus on the adhesive layer, as shown in Fig. 6. The camera shooting rate was 1 Hz. The collected images were input to an image processing toolkit, *ImageJ*, to post-analyze the recorded images and thus obtained the local separation of the crack tip "δ".

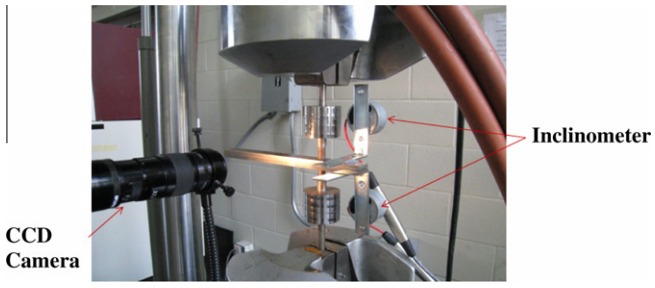

Fig. 6. DCB specimen attached with inclinometer during the peel test.

4. Test results and discussions

4.1. Global test results

The loading rate (at loading point) was equal to 1 μm/s. The preliminary studies showed that this rate could lead to a very stable descending branch when the crack was propagated, and it could be safely treated as a quasistatic loading condition. In the current study, a total of six groups of specimens which were numbered from group 1 to group 6 for the average adhesive thicknesses of 0.09, 0.2, 0.4, 0.6, 0.8, and 1 mm, respectively, were prepared and tested. Each group had 5 effective specimens, and a total of 30 effective specimens experienced the double cantilever beam (DCB) test by using the MTS 810 machine. The geometric parameters of each specimen are given in Table 1. Based on the analytical results of Ouyang and Li (2009a), with the current geometric configuration and the experimental data, it was found that all adherends (tool-grade steel) remained linear elastic during the entire test process without any plastic deformation. This indicates that all energy dissipations were contributed by cohesive fracture and plastic dissipations in the adhesive layer. A typical force vs. displacement curve (a specimen in group 2 with an adhesive thickness of 0.2 mm) at the loading point is shown in 7. The force linearly increases until the local damage occurs. The load nonlinearly increases until the crack initiation process is completed. After that, the crack tip starts propagating. A continuous drop in the peel

Table 1
Geometry of specimens.

Group number	Average adhesive thickness (mm)	Length (mm)	Height (mm)	Width (mm)	Initial crack length (mm)
1	0.09	254.10	6.35	25.41	52.12
2	0.2	254.11	6.35	25.44	52.22
3	0.4	254.09	6.34	25.42	52.18
4	0.6	254.08	6.35	25.39	52.44
5	0.8	254.10	6.36	25.46	52.37
6	1.0	254.08	6.35	25.37	52.11

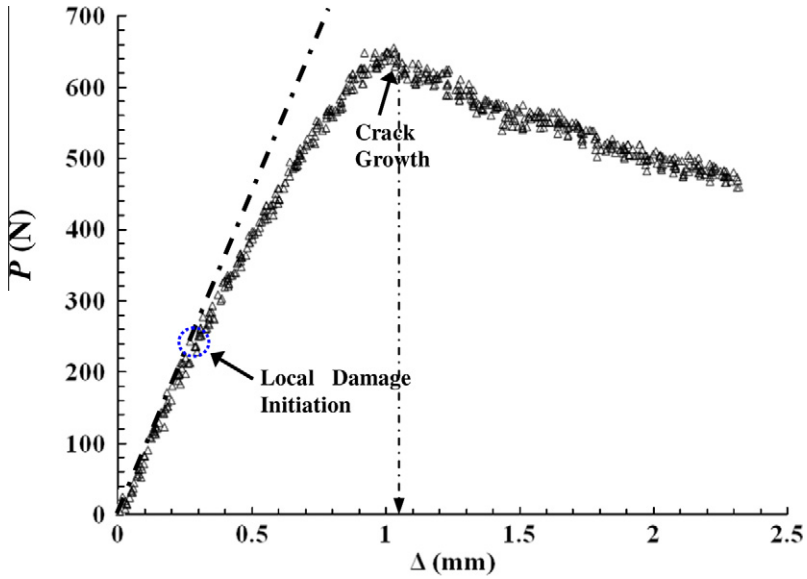

Fig. 7. A typical relationship between loadline displacements Δ and loadline peel force P for Group 2 (h_a = 0.2 mm).

force is seen as the crack continuously propagates until the crack reaches the DCB specimen's end.

Although there was no SEM, AFM or spectroscopy (XPS) examination of the morphology of the fractured surfaces, with the help of high resolution microscope, it was found that the failure mode was cohesive fracture for all cases. Even for the thinnest adhesive layer of 90 μm, an extremely thin adhesive layer was remained on the surfaces of the two separated adherends. It was thus believed that even for the thinnest layers, failure mode was still in the form of cohesive fracture instead of adhesive failure. This failure mode may be because the careful surface cleaning and treatment were conducted during the specimen preparation associated with the good bonding between the adhesive and adherends.

The data of the rotation angle at the loading point were collected by the inclinometer. A typical experimental curve between the rotation angle θ_P at the loadline and the displacement Δ at the loadline (a specimen in group 2 with thickness of 0.2 mm) is shown in Fig. 8. With Eq. (2), the experimental energy release rate J is determined by combining the measured θ_P and P (or combining Figs. 7 and 8). A typical relationship (a specimen in group 2 with thickness of 0.2 mm) between global energy release rate J and loadline displacement Δ is given in Fig. 9. In a real test, we found that it was fairly difficult to exactly define when the initial crack tip was propagated. Therefore, a characteristic strain energy release rate J_0 was defined which represented the J value when the maximum peel force P was reached. Note that with the growth of the crack, the global strain energy release rate keeps increasing as shown in Fig. 9 ($J - \Delta$ curve). This implies that the plastic dissipations beyond the crack tip must keep increasing during this stable growth process. However, the increase rate of J becomes slower and slower as the crack grows, which seems nearly stable even by the end of the test. Therefore, an approximate asymptote is added in Fig. 9 to estimate the interfacial toughness of the bonded joints. And this estimated asymptotic value is denoted by J_C or fracture energy.

4.2. Local test results

In this study, crack tip local deformations along the entire adhesive layer were recorded using the high resolution CCD camera. It

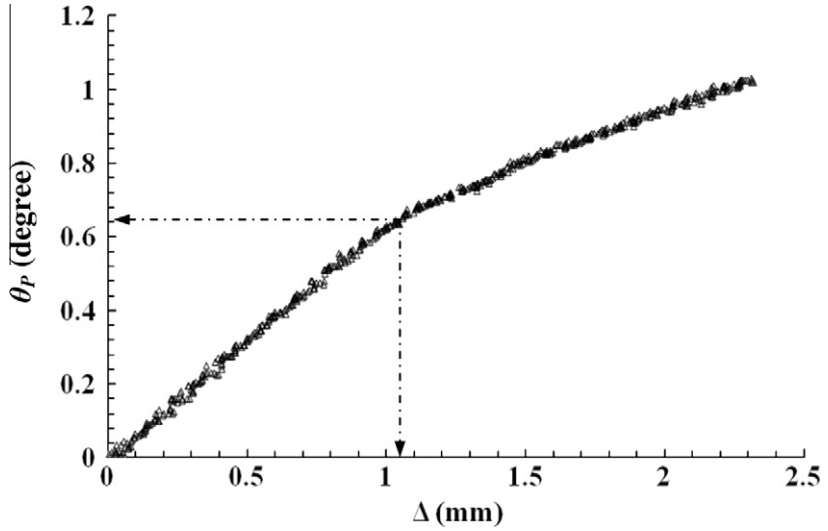

Fig. 8. A typical relationship between loadline displacements Δ and loadline rotation of adherend θ_P for Group 2 (h_a = 0.2 mm).

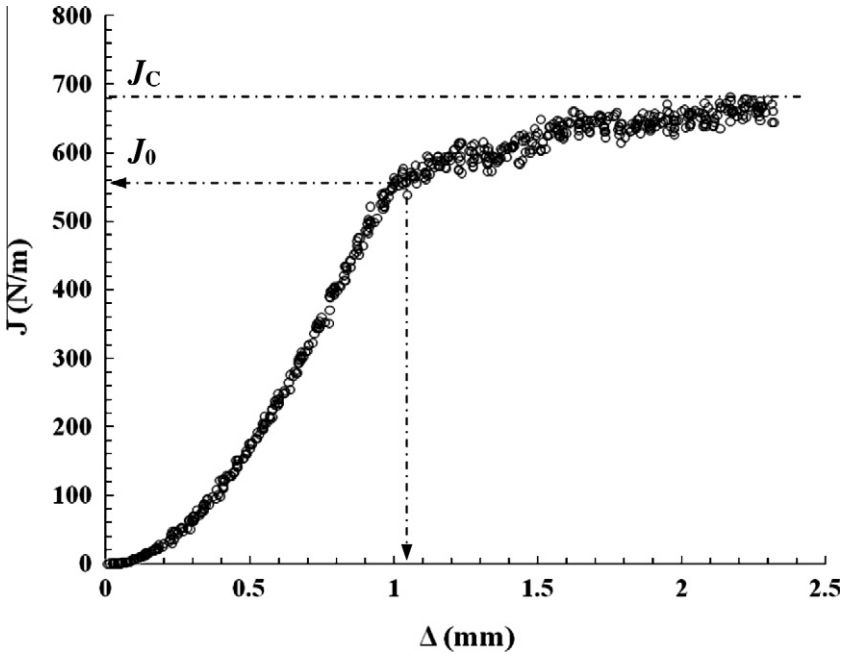

Fig. 9. A typical relationship between loadline displacements Δ and energy release rate J for Group 2 (h_a = 0.2 mm).

was also observed that a whitening zone appeared near the initial crack tip and was becoming more visible as the load was increased, as shown in Fig. 10. It was believed that the whitening zone consisted of numerous microcracks. When a lot of micro cracks were merged together and formed a macro crack, the initial crack started to propagate with the continuously increasing load. Digital images of the displacement field at the initial crack tip region were taken by the high resolution CCD camera. The value of the crack tip separation δ was measured as the relative normal displacement between the two adherends at the location of initial crack tip through the recorded digital images. Fig. 11 gives a typical relationship between the loadline displacement Δ (global displacement) and the local crack tip opening δ. By combining Figs. 9 and 11, a typical experimental $J-\delta$ curve was obtained as shown in Fig. 12 (a specimen in group 2 with thickness of 0.2 mm). Based on Eq. (3), the experimental $J-\delta$ curves were used to determine the equivalent interfacial traction-separation laws or $\sigma = \sigma(\delta)$ at different adhesive thicknesses.

4.3. Effects of the thickness of the adhesive layer

With the global test results of different groups, the average maximum peel loads P_{cr} of the five specimens in each group (with error bar) are plotted as a function of the adhesive thicknesses (0.09, 0.2, 0.4, 0.6, 0.8, and 1.0 mm) in Fig. 13. It can be observed that the average peak load is increased from 578.8 N (Group 1)

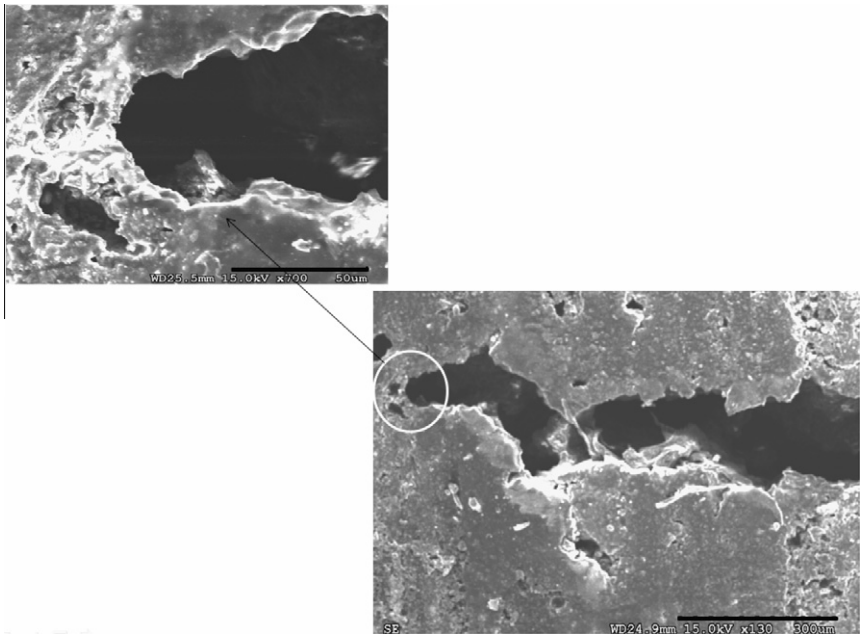

Fig. 10. Local plastic deformation as shown by the whitening region.

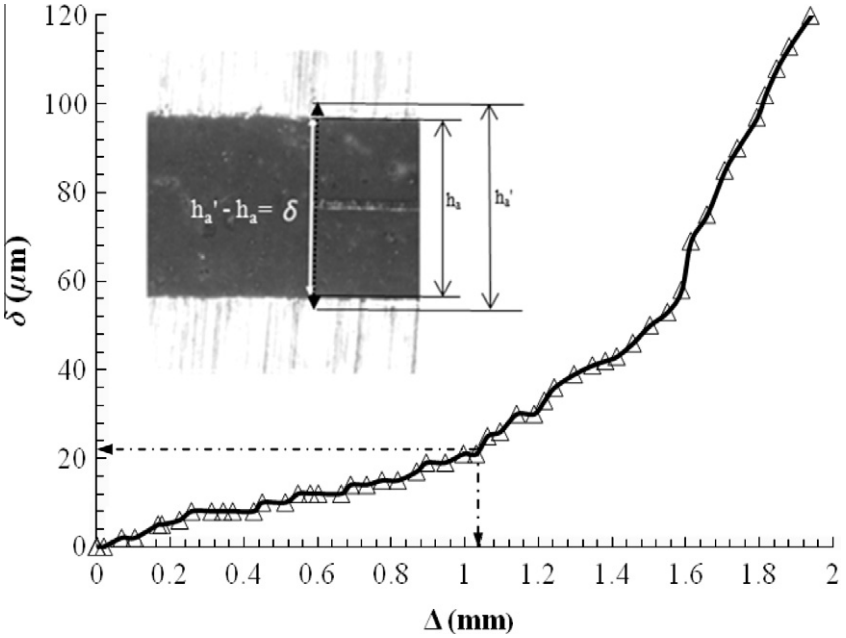

Fig. 11. A typical relationship between loadline displacements Δ and local crack tip separation δ for Group 2 (h_a = 0.2 mm).

to 791.12 N (Group 6) when the thickness of the adhesive layer increases (from 0.09 to 1.0 mm). These critical loads correspond to the characteristic energy release rate J_0. The average estimated fracture energy J_C (by the approximate asymptotes) and the average characteristic J_0 (at the maximum peel load) of the five specimens in each group (with error bar) are plotted as a function of the adhesive thickness in Fig. 14. One may see that the fracture energy J_C at the thickness of 0.09 mm is increased by approximately 160% when the adhesive thickness becomes 1.0 mm. The significant increase of J_0 and J_C are responsible for the increased load capacity when the adhesive thickness becomes thicker. Meanwhile, with Fig. 14, one may see that when the adhesive thickness is thin, J_0 and J_C are relatively close to each other. On the other hand, when it is relatively thick, J_0 and J_C are relatively departed from each other. Thus, we denote the difference between J_0 and J_C by $\Delta J = J_C - J_0$. Let's consider a parameter ξ, which represents the ratio of the average ΔJ over the pertinent average J_0 of the five specimens in each group. This ratio ξ is then plotted as a function of the adhesive thickness in Fig. 15. Obviously, the ratio ξ represents the relative increase in J to its initial value of J_0 as J value becomes a nearly stable value (J_C). Thus, Fig. 15 actually reflects the effects of adhesive thickness on the contributions by geometry a/h to the increase of plastic dissipations as crack grows.

After data collecting and curve-fitting process of the experimental $J-\delta$ curves, by applying Eq. (3), one can see that the interfacial traction-separation laws were determined by numerically differentiating the experimental $J-\delta$ curves. The cohesive law was calculated for each specimen. The typical equivalent cohesive law of each group is given in Fig. 16 at different adhesive thicknesses. From Fig. 16, one can see that three major effects of the adhesive thickness. First, the local characteristic separation (δ_0) corresponding to the interfacial strength σ_{max} decreases with the decrease of

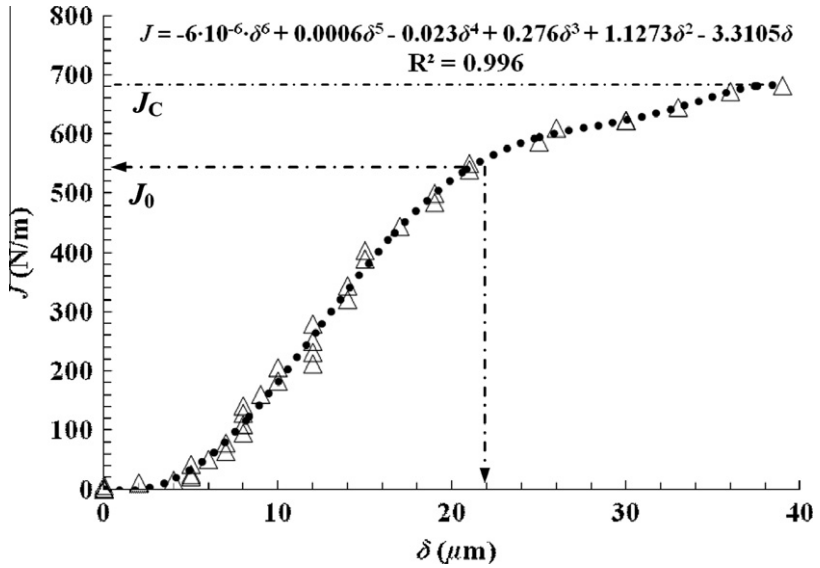

Fig. 12. A typical relationship between energy release rate J and local crack tip separation δ for Group 2 (h_a = 0.2 mm).

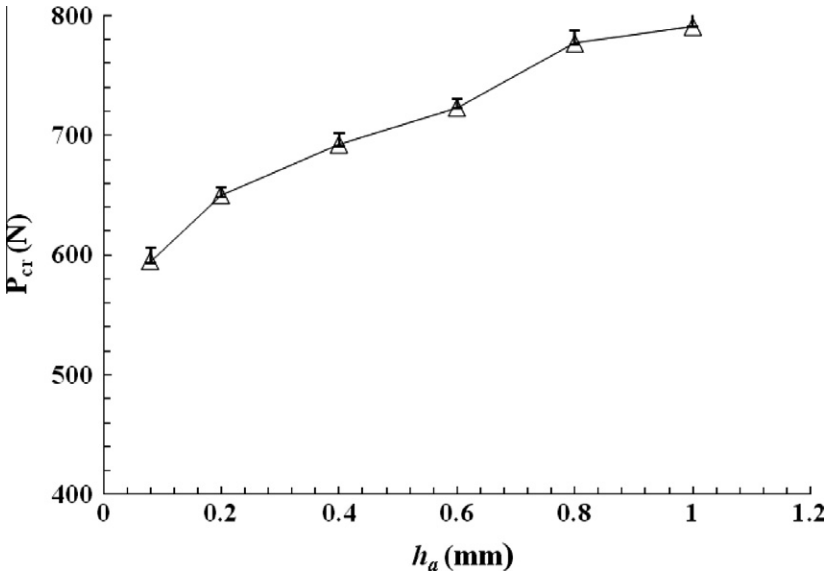

Fig. 13. The average maximum peel load P_{cr} at different adhesive thicknesses h_a.

the adhesive thickness. Second, the interfacial strength increases with the decrease of the adhesive thickness. Finally, the total area under the $\delta - \sigma$ curve, which represents the strain energy release rate at crack propagation, increases with the increase of the adhesive thickness. The complete thirty interfacial traction-separation laws (six groups at various adhesive thicknesses) are given in Fig. 17. One may see that the five specimens in each group (each adhesive thickness) present fairly consistent results.

The average interfacial strength σ_{max} of the six groups (with error bar) is plotted as a function of the adhesive thickness in Fig. 18. According to the manufacturer, the tensile strength of the bulk adhesive material is approximately 30.3 MPa (its yield strength is slightly lower than its tensile strength). One can see that the interfacial strength is 88 MPa at the thickness of 0.09 mm, which is approximately 3 times as large as the yield strength of the bulk adhesive material. The authors expect that with further decrease of the adhesive thickness, the measured equivalent interfacial strengths should keep increasing. On the contrary, with the increase of adhesive thickness, the measured interfacial strengths asymptotically approach a constant value. This asymptote seems being the yield strength of bulk adhesive material. Another phenomenon is that the equivalent interfacial strength seems increasing dramatically when the adhesive thickness was thinner than a certain value (such as 0.2 mm).

One may notice the turning point of the global loadline displacement in Fig. 7, which corresponds to the maximum load P_{cr}. For the sake of clarity, we denote it as Δ_0. In Fig. 8, Δ_0 corresponds to the turning point in loadline relative rotation θ_P. The same Δ_0 also corresponds to the turning point in the energy release rate in Fig. 9. All the above correspondences are regarding the global behaviors. In Fig. 11, the global loadline displacement Δ is correlated to the local crack tip opening δ. Note that in Fig. 11, Δ_0 is still corresponding to a turning point of the local opening, which is denoted by δ_0. According to this δ_0 in Fig. 11 ($\delta_0 \approx 22$ μm for the spec-

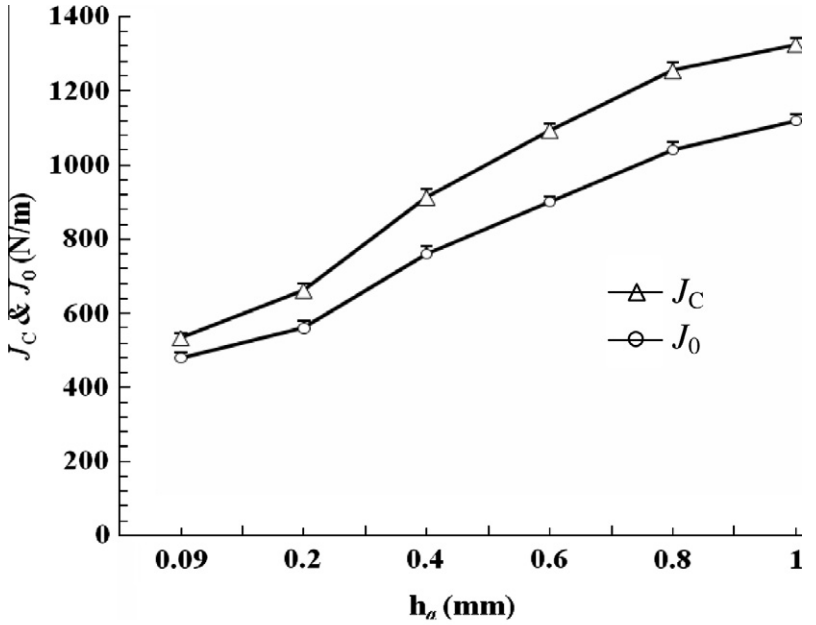

Fig. 14. The estimated fracture energy J_C and the characteristic energy release rate J_0 (corresponding to P_{cr}) with different adhesive thicknesses h_a.

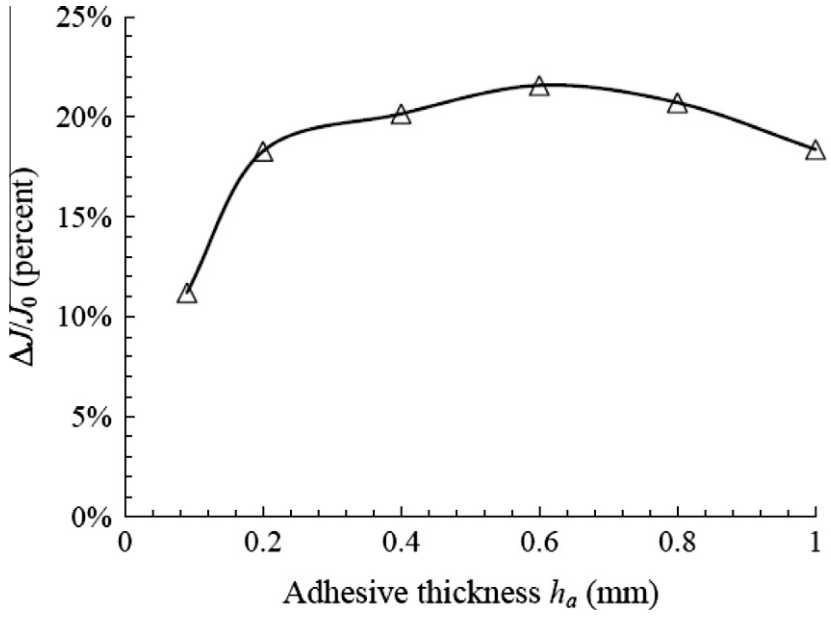

Fig. 15. The ratio of $\Delta J(\Delta J = J_C - J_0)$ over J_0 as a function of the adhesive thickness h_a.

imen with an adhesive thickness of 0.2 mm), one may find a corresponding J_0 in Fig. 12. Furthermore, one can see that this δ_0 corresponds to a certain interfacial stress which is not zero in Fig. 16. In other words, when the maximum peel load P_{cr} is reached, the crack tip opening δ is still smaller than its final separation δ_f. Our experimental observation regarding this phenomenon is thus consistent to the previous theoretical prediction (Ouyang and Li, 2009a).

5. Discussions and conclusions

Firstly, the global behaviors were investigated with different adhesive thicknesses in this experimental work. Due to the wide uses of modern toughened adhesives, the nonlinear zone beyond the crack tip usually may be comparable to the thickness of the bonded substrates. Instead of the linear elastic fracture mechanics (LEFM), the nonlinear fracture mechanics (NLLFM) was applied to consider the effects of root rotation which was caused by the relatively long plastic zone beyond the crack tip. As observed in the experiment, significant whitening and micro-cracking occurred before the crack tip propagated. Since the crack length during its growth was not recorded, *R*-curve was not available in this work. In order to examine the efficiency of the classical LEFM, the initial crack length $a_0 = 52$ mm and the corresponding maximum peel load P_{cr} (see Fig. 13) were used to calculate energy release rate. According to the classical LEFM (without root rotation corrections), the strain energy release rate (ERR) at the maximum load P_{cr} may be calculated by the first term $(Pa)^2/D$ in Eq. (2) by ignoring the second term $P\theta_0$. The energy release rate at the maximum load P_{cr} was also calculated by the NLFM according to the entire Eq. (2). The calculated values of J_0 are listed in Table 2 at various adhe-

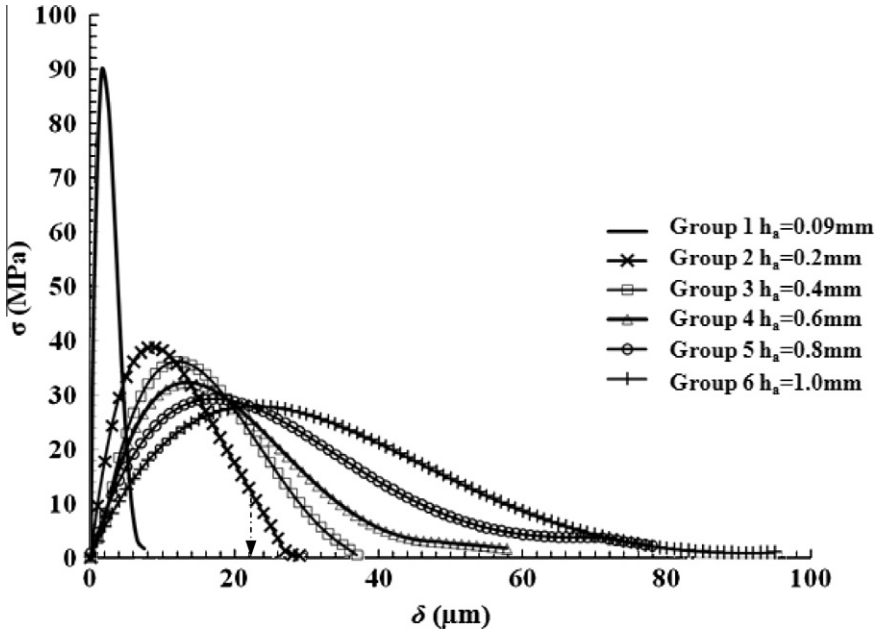

Fig. 16. Typical shape of the equivalent interfacial traction-separation laws with different thicknesses of adhesive layer.

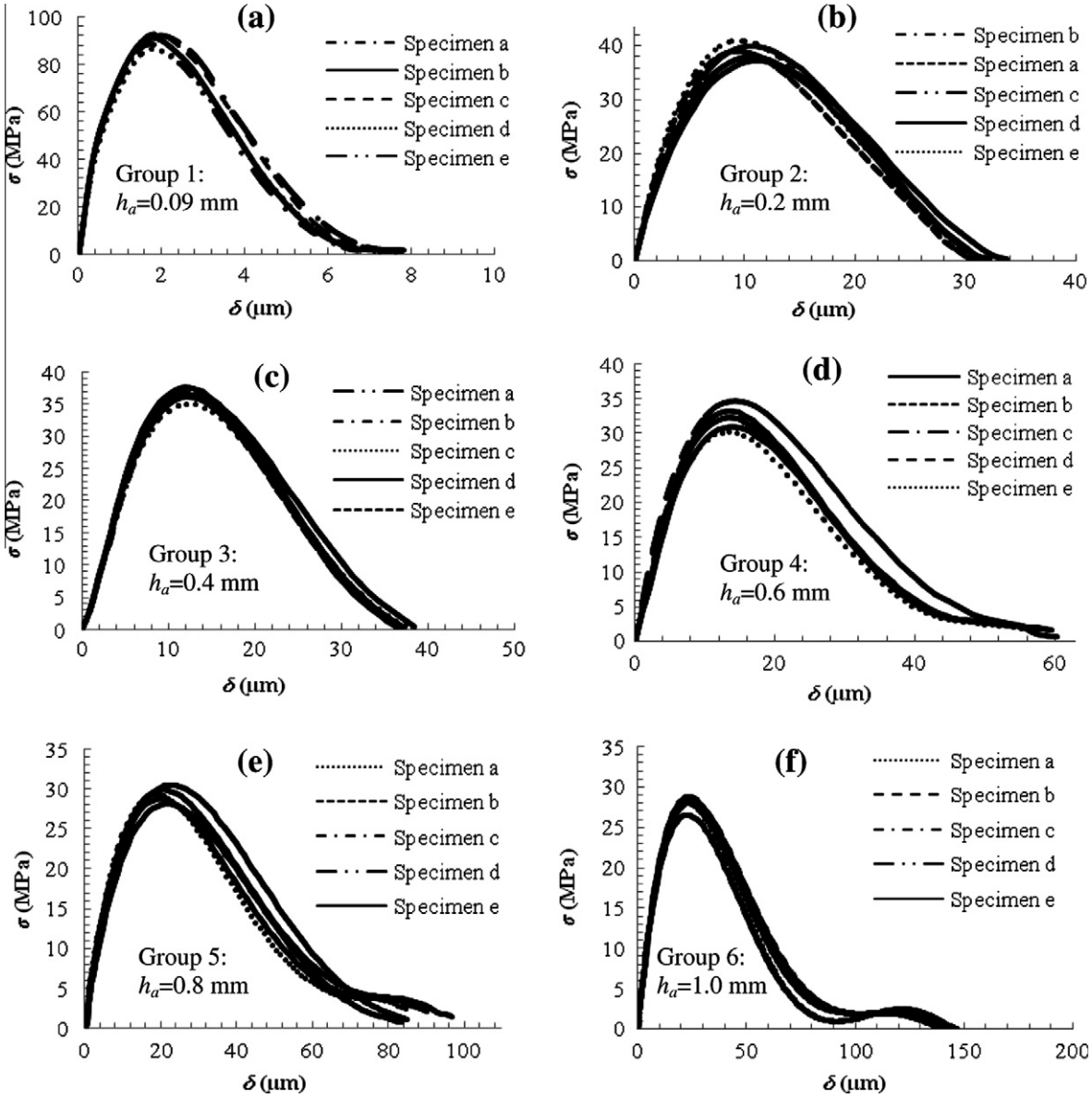

Fig. 17. The shapes of all equivalent interfacial traction-separation laws with different thicknesses of adhesive layer: (a) adhesive thickness h_a = 0.09 mm; (b) adhesive thickness h_a = 0.2 mm; (c) adhesive thickness h_a = 0.4 mm; (d) adhesive thickness h_a = 0.6 mm; (e) adhesive thickness h_a = 0.8 mm; (f) adhesive thickness h_a = 1.0 mm.

sive thicknesses. Note that $a_0/h \approx 8.2$, which can be considered as a slender "cantilever beam". Even for such a case, the root rotation effects are significant due to cohesive fracture and plastic deformation beyond the crack tip. For instance, the LEFM prediction deviates nearly 70% from the NLFM prediction with the typical moderate thickness h_a = 0.4 mm. It is worth noting, the deviations should be even slightly larger with the growth of crack, since the tests showed that the J values kept increasing with crack growth due to increased plastic dissipations. The ratio of the calculated J_0 values by NLFM over that by LEFM was denoted by η and plotted as a function of the adhesive thickness in Fig. 19. One can see that the huge difference between the LEFM and NLFM at various adhesive thicknesses.

Meanwhile, the local behaviors were studied with different adhesive thicknesses. An accurately calibrated numerical model should not only be able to predict the global displacement, but also predict the local separation δ. Based on the correspondence in Figs. 9 and 11, one can further find the correspondence between δ and J_0 as shown in Fig. 12. Since the $J_0 - \delta$ curves simultaneously include the information of global rotation, global force and local separation, it is even stricter than Fig. 11 for parameter calibrations. In a numerical simulation, it is not difficult to find the global peel force, loadline rotation, and local crack tip opening between the two adherends. In other words, with the output of a FEM modeling (embedded with the parameters to be calibrated), one may obtain the numerical $J_0 - \delta$ curves. The differentiation of these curves gives the equivalent interfacial traction-separation laws. By repeating this process at different adhesive thickness, one may have a series of thickness dependent interfacial traction-separation laws. Finally, one may compare these numerical laws to the experimentally measured laws (see Fig. 17) at various adhesive thicknesses. The authors believe that this proposed method should be able to give accurately calibrated parameters for a numerical model. Compared to the traditional global calibration method, this method may offer much more direct and reliable results. Note that in a real test, it is very difficult to measure the local full field stress or strain distributions in the thin interlayer even with the photoelasticity technique due to the significant plastic deformations.

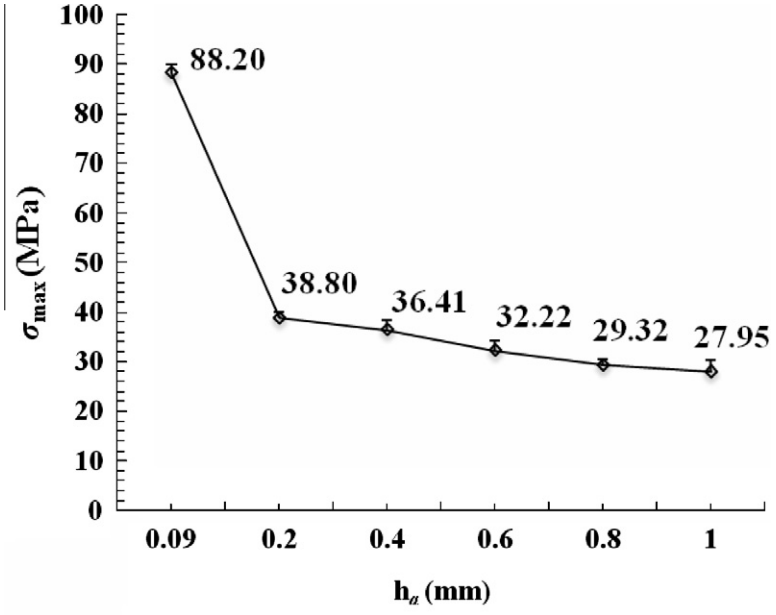

Fig. 18. The effect of the adhesive thickness on the interfacial strength σ_{max}.

Table 2
Comparisons of the calculated energy release rate J_0 corresponding to the maximum peel load P_{cr} by NLFM and classical LEFM (without root rotation corrections), respectively.

Average adhesive thickness h_a (mm)	Adherend thickness h (mm)	Initial crack length a_0 (mm)	LEFM J_0 (N/m)	Nonlinear J_0 (N/m)	Ratio of J_0(N/L)
0.09	6.35	52.12	0.335	0.48	143.2%
0.2	6.35	52.22	0.406	0.56	137.9%
0.4	6.34	52.18	0.450	0.76	168.6%
0.6	6.35	52.44	0.501	0.90	179.6%
0.8	6.36	52.37	0.574	1.04	181.2%
1.0	6.35	52.11	0.597	1.12	187.6%

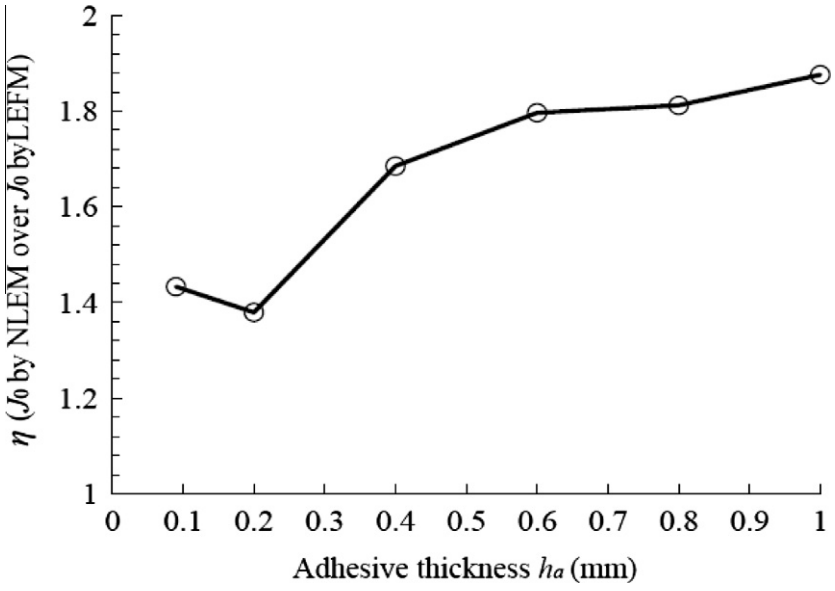

Fig. 19. The ratio of the calculated J_0 by NLFM over that by LEFM as a function of the adhesive thickness h_a.

Our method may possess the potential to be considered as a feasible option.

Finally, it is noted that the measured cohesive law ($\sigma - \delta$) in Figs. 16 and 17 is based on the indirect method (by taking derivative of the experimental $J - \delta$ curve in Fig. 12). One may ask the error transferred by differential. Unfortunately, without the true $J - \delta$ curve or the direct experimental data of cohesive law ($\sigma - \delta$ curve), it is extremely difficult to define and calculate the actual error of

the cohesive law in Figs. 16 and 17. The curve-fitting equation and its R^2 value of the experimental $J-\delta$ data are given in Fig. 12 to define the error of J. It is seen that the error of the curve-fitting is quite small. Further work is required to explore the direct measurement of $\sigma-\delta$, which remains a challenge for the interfacial fracture problem.

In summary, the plastic dissipations in modern toughened adhesive interlayer are quite common. Due to these realistic demands, the thicknesses of the adhesive layer play an important role (although they are still relatively thin). CZMs based numerical and analytical models may offer a powerful means to consider the significant nonlinear fracture behaviors of modern adhesively bonded joints. However, the parameters in these models need careful calibrations by experimental data in order to accurately simulate the failure process. Specially, the tests are highly preferred to be conducted with various typical adhesive thicknesses, so that the numerical and analytical models can be calibrated with different adhesive thicknesses. The local cohesive separation and plastic deformation across the adhesive layer is very complex. Thus, it is possible that the integrated behavior of cohesive separations and plastic deformations across the interlayer may have largely identical global responses even though their local behaviors are completely different. Therefore, the cross-calibrations by local and global test may possess a huge potential for the accurate parameter characterizations. Compared to the widely investigated global behaviors, fewer attentions have been paid to the local test ($\delta-J$ curves and interfacial traction-separation laws). Among the limited local tests, most of them were conducted with a fixed adhesive thickness. Motivated by such a situation, this work presented the global and local tests of the interfacial fracture with various typical adhesive thicknesses. Our test results may provide valuable data regarding the effects of the adhesive thickness for the research communities, and offer useful references for the future numerical and analytical models.

Acknowledgements

This study is based upon work supported by the NSF under Grant No. NSF/CMMI0900064 and by the NASA/EPSCoR under Grant No. NASA/LEQSF (2007-10)-Phase3-01. The authors are grateful for the support by LONI Project under the Grant No. LEQSF (2007-12)-ENH-PKSFI-PRS-01 (Subcontract No. 17120).

References

Alfano, G., Crisfield, M.A., 2001. Finite element interface models for the delamination analysis of laminated composites: mechanical and computational issues. International Journal of Numerical Methods in Engineering 50, 1701–1736.

Andersson, T., Stigh, U., 2004. The stress-elongation relation for an adhesive layer loaded in peel using equilibrium and energetic forces. International Journal of Solids and Structures 41, 413–434.

Andruet, R.H., Dillard, D.A., Holzer, S.M., 2001. Two- and three-dimensional geometrical nonlinear finite elements for analysis of adhesive joints. International Journal of Adhesion and Adhesives 21, 17–34.

Barenblatt, G.I., 1959. The formation of equilibrium cracks during brittle fracture. General ideas and hypothesis. Axisymmetrical cracks. Journal of Applied Mathematics and Mechanics (PMM) 23, 622–636 (English translation).

Blackman, B.R.K., Hadavinia, H., Kinloch, A.J., Williams, J.G., 2003. The use of a cohesive zone model to study the fracture of fibre composites and adhesively-bonded joints. International Journal of Fracture 119, 25–46.

Camacho, G.T., Ortiz, M., 1996. Computational modeling of impact damage in brittle materials. International Journal of Solids and Structures 33, 2899–2938.

Chai, H., 1988. Shear fracture. International Journal of Fracture 37, 137–159.

Chai, H., 1995. Deformation and fracture of particulate epoxy in adhesive bonds. Acta Metallurgica Materialia 43, 163–172.

Chowdhury, S.R., Narasimhan, R., 2000. A finite element analysis of stationary crack tip fields in a pressure sensitive constrained ductile layer. International Journal of Solids and Structures 37, 3079–3100.

Corigliano, A., 1993. Formulation, identification and use of interface models in the numerical analysis of composite delamination. International Journal of Solids and Structures 30, 2779–2811.

Dugdale, D.S., 1960. Yielding of steel sheets containing slits. Journal of the Mechanics and Physics of Solids 8, 100–104.

Hillerborg, A., Modéer, M., Petersson, P.E., 1976. Analysis of crack formation and crack growth in concrete by means of fracture mechanics and finite elements. Cement and Concrete Research 6, 773–782.

Högberg, J.L., 2006. Mixed mode cohesive law. International Journal of Fracture 141, 549–559.

Högberg, J.L., Sørensen, B.F., Stigh, U., 2007. Constitutive behaviour of mixed mode loaded adhesive layer. International Journal of Solids and Structures 44, 8335–8354.

Hutchinson, J.W., Evans, A.G., 2000. Mechanics of materials: top-down approaches to fracture. Acta Materialia 48, 125–135.

Ikeda, T., Yamashita, A., Lee, D., Miyazaki, N., 2000. Failure of a ductile adhesive layer constrained by hard adherends. Journal of Engineering Materials and Technology 122, 80–85.

Kafkalidis, M.S., Thouless, M.D., Yang, Q.D., Ward, S.M., 2000. Deformation and fracture of adhesive layers constrained by plastically-deforming adherends. Journal of Adhesion Science and Technology 14, 1593–1607.

Kinloch, A.J., Shaw, S.J., 1981. The fracture resistance of a toughened epoxy adhesive. Journal of Adhesion 12, 59–77.

Klarbring, A., 1991. Derivation of a model of adhesively bonded joints by the asymptotic expansion method. International Journal of Engineering Science 29, 493–512.

Lee, D.B., Ikeda, T., Miyazaki, N., Choi, N.S., 2004. Effect of bond thickness on the fracture toughness of adhesive joints. Journal of Engineering Materials and Technology 126, 14–18.

Leffler, K., Alfredsson, K.S., Stigh, U., 2007. Shear behaviour of adhesive layers. International Journal of Solids and Structures 44, 520–545.

Lorenzis, L.D., Zavarise, G., 2009. Cohesive zone modeling of interfacial stresses in plated beams. International Journal of Solids and Structures 46, 4181–4191.

Madhusudhana, K.S., Narasimhan, R., 2002. Experimental and numerical investigations of mixed mode crack growth resistance of a ductile adhesive joint. Engineering Fracture Mechanics 69, 865–883.

Moura, M.F.S.F., de Campilho, R.D.S.G., Gonçalves, J.P.M., 2009. Pure mode II fracture characterization of composite bonded joints. International Journal of Solids and Structures 46, 1589–1595.

Needleman, A., 1987. A continuum model for void nucleation by inclusion debonding. ASME Journal of Applied Mechanics 54, 525–531.

Nguyen, C., Levy, A.L., 2009. An exact theory of interfacial debonding in layered elastic composites. International Journal of Solids and Structures 46, 2712–2723.

Ouyang, Z., Li, G., 2009a. Local damage evolution of DCB specimens during crack initiation process: a natural boundary condition based method. ASME Journal of Applied Mechanics 76, 051003-1–051003-8.

Ouyang, Z., Li, G., 2009b. Nonlinear interface shear fracture of end notched flexure specimens. International Journal of Solids and Structures 46, 2659–2668.

Ouyang, Z., Li, G., 2009c. Cohesive zone model based analytical solutions for adhesively bonded pipe joints under torsional loading. International Journal of Solids and Structures 46, 205–1217.

Ouyang, Z., Li, G., 2009d. Interfacial debonding of pipe joints under torsion loads: a model for arbitrary nonlinear cohesive laws. International Journal of Fracture 155, 19–31.

Pan, J., Leung, C.K.Y., 2007. Debonding along the FRP-concrete interface under combined pulling/peeling effects. Engineering Fracture Mechanics 74, 132–150.

Pardoen, T., Ferracin, T., Landis, C.M., Delannay, F., 2005. Constraint effects in adhesive joint fracture. Journal of the Mechanics and Physics of Solids 53, 1951–1983.

Parrinello, F., Failla, B., Borino, G., 2009. Cohesive–frictional interface constitutive model. International Journal of Solids and Structures 46, 2680–2692.

Rice, J.R., 1968. A path independent integral and the approximate analysis of strain concentration by notches and cracks. Journal of Applied Mechanics 35, 379–386.

Rose, J.H., Smith, J.R., Ferrante, J., 1983. Universal features of bonding in metals. Physical Review B 28, 1835–1845.

Salomonsson, K., Andersson, T., 2008. Modeling and parameter calibration of an adhesive layer at the meso level. Mechanics of Materials 40, 48–65.

Sørensen, B.F., 2002. Cohesive law and notch sensitivity of adhesive joints. Acta Materialia 50, 1053–1061.

Tvergaard, V., 1990. Effect of fibre debonding in a whisker-reinforced metal. Material Science and Engineering A 125, 203–213.

Tvergaard, V., Hutchinson, J.W., 1992. The relation between crack growth resistance and fracture process parameters in elastic–plastic solids. Journal of the Mechanics and Physics of Solids 40, 1377–1397.

Tvergaard, V., Hutchinson, J.W., 1996. On the toughness of ductile adhesive joints. Journal of the Mechanics and Physics of Solids 44, 789–800.

Wei, Y., Hutchinson, J.W., 1998. Interface strength, work of adhesion and plasticity in the peel test. International Journal of Fracture 93, 315–333.

Williams, M.L., 1959. The stress around a fault or crack in dissimilar media. Bulletin of the Seismological Society of America 49, 199–204.

Williams, J.G., Hadavinia, H., 2002. Analytical solutions for cohesive zone models. Journal of the Mechanics and Physics of Solids 50, 809–825.

Xu, X.P., Needleman, A., 1993. Void nucleation by inclusion debonding in a crystal matrix. Modeling and Simulation in Materials Science and Engineering 1, 111–132.

Yan, Y., Shang, F., 2009. Cohesive zone modeling of interfacial delamination in PZT thin films. International Journal of Solids and Structures 46, 2739–2749.
Yan, C., Mai, Y.W., Ye, L., 2001. Effect of bond thickness on fracture behaviour in adhesive joints. The Journal of Adhesion 75, 27–44.
Yang, Q.D., Thouless, M.D., Ward, S.M., 2001a. Elastic–plastic Mode-II fracture of adhesive joints. International Journal of Solids and Structures 38, 3251–3262.
Yang, Q.D., Thouless, M.D., Ward, S.M., 2001b. Mixed mode fracture analysis of plastically-deforming adhesive joints. International Journal of Fracture 110, 175–187.
Zhu, Y., Liechti, K.M., Ravi-Chandar, K., 2009. Direct extraction of rate-dependent traction-separation laws for polyurea/steel interfaces. International Journal of Solids and Structures 46, 31–51.